Precision Guidance for Mars Entry with a Supersonic Inflatable Aerodynamic Decelerator

Zixuan Liang*
Beihang University, Beijing, 100191, People's Republic of China

and

Kenneth D. Mease†
University of California, Irvine, Irvine, California, 92697

I. Introduction

In 2012, the atmospheric entry of the Mars Science Laboratory (MSL) was guided, enabling unprecedented Mars landing accuracy. The MSL rover Curiosity is nearly 900 kg which is the largest landed mass to date. For the future Mars Sample Return (MSR) mission, a landed mass double that of Curiosity's, and similar, if not greater, landing accuracy will be required [1]. The decelerator required for larger mass can be achieved either by increasing the drag area or by propulsive braking; the former is considered in this Note.

To increase the drag area and still meet launch vehicle constraints, a hypersonic inflatable aerodynamic decelerator (HIAD) and a supersonic inflatable aerodynamic decelerator (SIAD) are being investigated for future Mars missions [2-6]. One part of the low density supersonic decelerator (LDSD) system, the SIAD, had two test flights, one in 2014 and the other in 2015 [7-9]. In the testing, though the parachute was damaged, the SIAD performed well. The SIAD is deployed at about Mach 4 during the entry phase. The purpose of this Note is to develop an appropriate guidance method for Mars entry with a SIAD.

Some previous guidance methods for Mars entry rely on a pre-designed reference trajectory. In [10-14], the reference trajectory is tracked to fly the vehicle to the target. MSL employed neighboring optimal guidance, derived for the linearized dynamics about a reference trajectory. The SIAD deployment is expected to be completed in one second [8]. When the vehicle's diameter increases from 4.5 m for the MSL-type aeroshell to 6 m for the SIAD [3], the reference area and the drag would increase abruptly by about 78%. The use of a SIAD thus poses two problems

* Postdoctoral Fellow, School of Astronautics, and Visiting Scholar, University of California, Irvine; aliang@buaa.edu.cn. Current affiliation: Beijing Institute of Technology.
† Professor, Department of Mechanical and Aerospace Engineering; kmease@uci.edu. Associate Fellow AIAA.

for reference trajectory-based guidance: (1) the deployment event creates a near-discontinuity in the entry dynamics and (2) for a control-limited entry vehicle, the timing of the deployment is a beneficial guidance parameter and should not be pre-designed. Therefore, a numerical predictor-corrector approach, see [15-17] for example, that does not rely on a reference trajectory is a better choice for Mars entry with a SIAD. A predictor-corrector approach for Mars entry is investigated by Putnam and Braun [18] to control the drag-skirt jettison time which is also a discrete-event. In contrast to the SIAD, the drag-skirt is jettisoned during the entry to reduce the reference area. Similarly in [19], a jettison guidance algorithm based on the predictor-corrector is used for the planetary aerocapture. In [20], the discrete-event drag modulation approach is expanded to three options: single-stage jettison systems, two-stage jettison systems, and continuously variable systems.

In the predictor-corrector approach, the flight dynamics are numerically integrated to predict the terminal state. Then, the guidance parameters are adjusted to null the error between the predicted and required terminal states. With faster processors, the predictor-corrector guidance is feasible, but considering the reliability, the number of guidance parameters must be small. In [17, 21], the bank angle profile is parameterized by a linear function or even a constant such that a single guidance parameter is adjusted. Recently, Lu et al. [22] verified the Fully Numerical Predictor-corrector Entry Guidance (FNPEG) for both direct and skip entry missions. In order to satisfy the acceleration constraint for Mars entry, Zheng et al. [23] developed a constrained predictor-corrector algorithm based on an exact-penalty method. Similarly, a single guidance parameter is updated onboard.

In this Note, a predictor-corrector entry guidance algorithm is developed for the longitudinal guidance of an MSL-type vehicle with a SIAD and a heavier payload. In contrast to Lu's work [17, 21, 22], the proposed algorithm takes the SIAD deployment Mach number as an additional guidance parameter. A weighted parachute box is designed to evaluate the terminal condition given by the predictor. This box provides the score for the parachute deployment condition. The guidance algorithm aims to maximize the score by adjusting the bank angle profile and the SIAD deployment Mach number in the corrector step. Thus, the proposed guidance method does not rely on either a pre-designed reference trajectory or a fixed SIAD deployment Mach number. The lateral guidance is accomplished using previously developed bank reversal logic [24]. A range trigger, which has been found to be effective for the landing accuracy improvement [14, 18, 25-27], is employed for the parachute deployment. The performance of the Mars entry guidance algorithm is assessed for various cases by numerical simulations.

II. Modeling Mars Entry with a SIAD

A schematic for Mars entry with a SIAD is shown in Fig. 1. In the hypersonic phase, the aeroshell is used for deceleration. Then, in the supersonic phase, the SIAD deploys at a specified Mach number. After this deployment, the vehicle's diameter increases. Finally, the parachute is deployed when constraints for the Mach number and the dynamic pressure are satisfied. The guidance system should guarantee that a desirable deployment condition for the parachute is achieved at the end of the entry phase.

The ballistic coefficient which affects the entry trajectory is

$$\beta = \frac{m}{S_A C_D} \tag{1}$$

where m is the mass of the vehicle, S_A is the reference area, and C_D is the drag coefficient.

The vehicle's reference area increases when the SIAD is pressurized. According to Eq. (1), a larger S_A would result in a lower β, which provides higher deceleration. In addition, Eq. (1) also indicates that a larger S_A allows the same β for a greater m. Thus, the SIAD can be used to land high-mass payloads on Mars. In this Note, details for the SIAD structure are neglected, and the guidance algorithm focuses mainly on the impact of the aerodynamic forces on the flight trajectory.

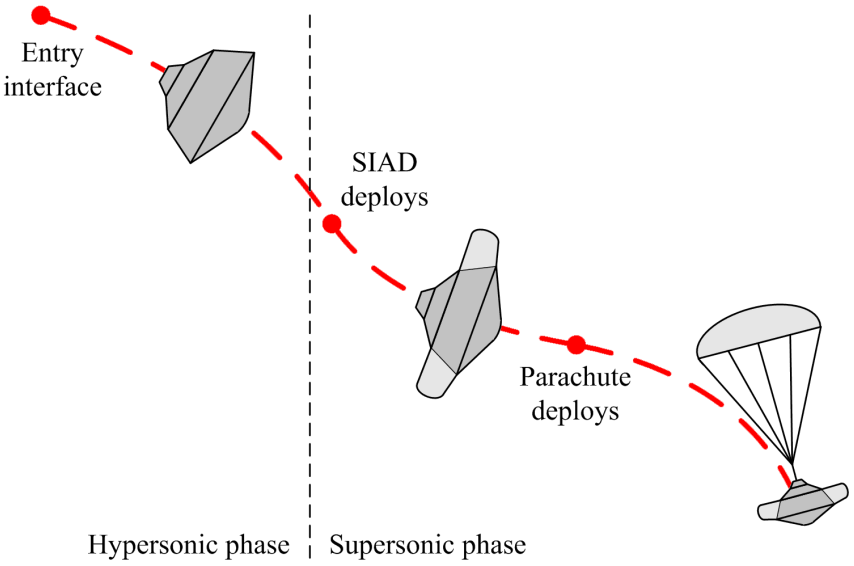

Fig. 1 Schematic for Mars entry with a SIAD

The point-mass dynamics of an entry vehicle with respect to a planet-fixed rotating coordinate frame are [28]

$$\dot{r} = v \sin\gamma \tag{2}$$

$$\dot{\theta} = \frac{v \cos\gamma \cos\psi}{r \cos\phi} \tag{3}$$

$$\dot{\phi} = \frac{v \cos\gamma \sin\psi}{r} \tag{4}$$

$$\dot{v} = -\frac{D}{m} - g \sin\gamma + \omega^2 r \cos\phi (\sin\gamma \cos\phi - \cos\gamma \sin\phi \sin\psi) \tag{5}$$

$$\dot{\gamma} = \frac{1}{v}\left[\frac{L \cos\sigma}{m} - g \cos\gamma + \frac{v^2 \cos\gamma}{r} + 2\omega v \cos\phi \cos\psi + \omega^2 r \cos\phi (\cos\gamma \cos\phi + \sin\gamma \sin\phi \sin\psi)\right] \tag{6}$$

$$\dot{\psi} = -\frac{1}{v}\left[\frac{L \sin\sigma}{m \cos\gamma} + \frac{v^2 \cos\gamma \cos\psi \tan\phi}{r} - 2\omega v (\tan\gamma \cos\phi \sin\psi - \sin\phi) + \frac{\omega^2 r}{\cos\gamma} \sin\phi \cos\phi \cos\psi\right] \tag{7}$$

where r is the radial distance from the Mars center to the vehicle, θ is the longitude, ϕ is the latitude, v is the velocity magnitude, γ is the flight-path angle, ψ is the velocity heading angle, σ is the bank angle, ω is the Mars rotation rate, and g is the gravitational acceleration. The lift force L and the drag force D are given by

$$\begin{cases} L = \frac{1}{2}\rho v^2 S_A C_L \\ D = \frac{1}{2}\rho v^2 S_A C_D \end{cases} \tag{8}$$

where ρ is the atmospheric density, and C_L is the lift coefficient.

The parameter M_{SIAD} is defined as the Mach number for the SIAD deployment. The SIAD is expected to pressurize when $M_{\mathrm{SIAD}} \leq 5$ such that the aerothermal heating can be neglected [2]. Additionally, deployment at $M_{\mathrm{SIAD}} < 3$ is likely to bring oscillations [4]. Therefore, a reasonable deployment condition for the SIAD is $3 \leq M_{\mathrm{SIAD}} \leq 5$. In the flight test of the LDSD [7], the deployment Mach number is $M_{\mathrm{SIAD}} = 4$. However, a fixed deployment condition for the SIAD would eliminate a significant means of controlling the entry flight. Thus, along with the bank angle, M_{SIAD} is used as a guidance parameter.

III. Guidance Approach

A. Objective and Strategy

The entry guidance objective is to deliver the vehicle to a specified longitude and latitude with sufficient accuracy and an acceptable parachute deployment condition. The controls commanded by the guidance logic are the bank angle, the SIAD deployment, and the parachute deployment. In the proposed guidance logic, bank reversal logic commands the bank angle sign and a predictor-corrector algorithm commands the bank angle magnitude and

the SIAD deployment. A range trigger commands parachute deployment. In the rest of this section, the details of the proposed guidance are presented.

B. Lateral Guidance

Bank reversal logic provides the sign of the bank angle according to a heading error corridor [24]. The corridor boundary $\Delta_\psi(v)$ is designed by a function of the velocity and given by

$$\Delta_\psi(v) = \begin{cases} c_1, & \text{if } v > v_1 \\ c_2 + (c_1 - c_2)\dfrac{v}{v_1}, & \text{if } v \le v_1 \end{cases} \tag{9}$$

where c_1 and c_2 are positive constant, and v_1 is a specified velocity between the initial and terminal values. For the numerical results in this Note, we use c_1 = 4 deg, c_2 = 1 deg, and v_1 = 1500 m/s.

With the corridor boundary, the bank reversal logic is as follows: if the heading error is greater than $\Delta_\psi(v)$, the bank angle is reversed to positive; if the heading error is less than $-\Delta_\psi(v)$, the bank angle is reversed to negative; otherwise, the bank angle sign is unchanged from the previous cycle.

C. Weighted Parachute Box for Longitudinal Guidance

The deployment state for the parachute is constrained in Mach number, dynamic pressure, and altitude. The constraints are expressed as

$$M_{\min} \le M_{\mathrm{P}} \le M_{\max} \tag{10}$$

$$\bar{q}_{\min} \le \bar{q}_{\mathrm{P}} \le \bar{q}_{\max} \tag{11}$$

$$h_{\mathrm{P}} \ge h_{\min} \tag{12}$$

where $M_{\min}$ and $M_{\max}$ are the minimum and maximum Mach number, $\bar{q}_{\min}$ and $\bar{q}_{\max}$ are the minimum and maximum dynamic pressure, and $h_{\min}$ is the minimum altitude. The minimum altitude is set to provide sufficient room for the subsequent descent and landing phases.

Generally the constraints in Eqs. (10-12) are expressed as a box for the vehicle's altitude and velocity, using nominal models for the speed of sound and atmospheric density [1]. The parachute box is approximately a pentagon. Assume the parachute constraints are specified by $M_{\min}$ = 1.4, $M_{\max}$ = 2.2, $\bar{q}_{\min}$ = 300 Pa, $\bar{q}_{\max}$ = 850 Pa, and $h_{\min}$ = 6 km [29]. The corresponding parachute box is shown in Fig. 2. Point P is a nominal parachute deployment condition, selected as in the centroid of the parachute box to provide margin for guidance and navigation errors.

The guidance system should deliver the vehicle to a deployment state within the parachute box. Letting T denote the deployment state, a scoring function is defined as

$$C(\mathrm{T}) = 1 - \frac{|\mathrm{PT}|}{|\mathrm{PB}|} \tag{13}$$

where point B is the boundary point along the extension of line segment PT as shown in Fig. 2. It follows that C(P) = 1, and for every boundary point, C(T) = 0. For any point outside the box, the score is negative. Thus, the scoring function provides a measure of how accurately the vehicle is delivered to the point P of the parachute box and whether or not the delivery point T is within the parachute box.

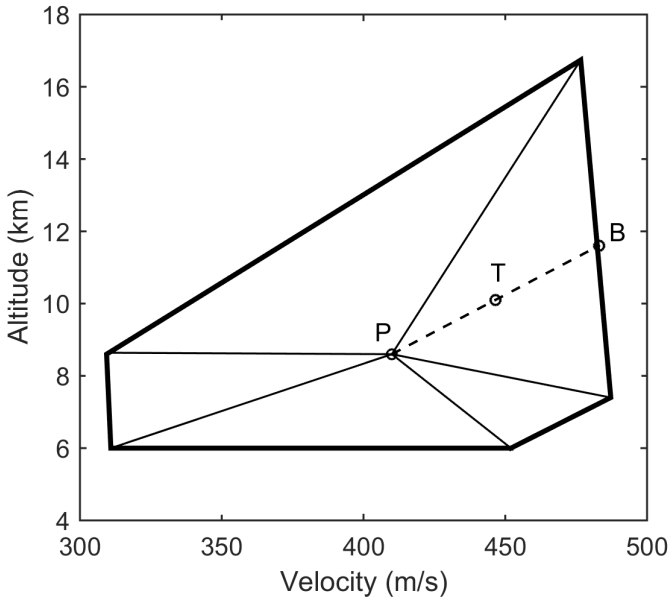

Fig. 2 Parachute box

A weighted parachute box with reference scores is illustrated in Fig. 3. In the next subsection, the predictor-corrector guidance algorithm is designed based on the weighted parachute box which provides scores for the predicted terminal conditions.

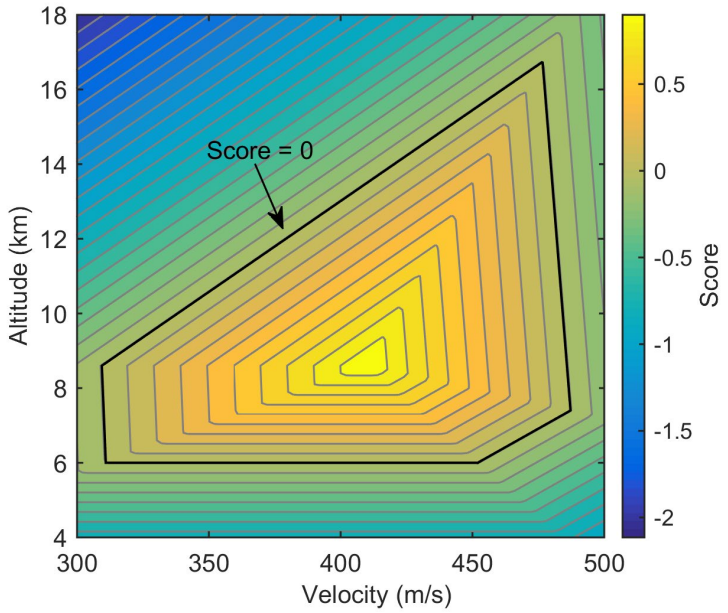

Fig. 3 Weighted parachute box with reference scores

D. Predictor-Corrector Longitudinal Guidance

For the numerical predictor-corrector algorithm, the flight dynamics given by Eqs. (2-7) are integrated with the current bank angle profile, SIAD deployment Mach number, and the bank angle sign determined by the bank reversal logic. Bank reversals are modeled as maximum bank rate and acceleration maneuvers. If, at the current guidance update, a bank reversal is commanded, the longitudinal predictor-corrector algorithm pauses. Once the reversal is completed, the predictor-corrector algorithm resumes. The trajectory integration is always terminated when the range to the target is a minimum [25, 26]. The range to the target is computed using the great-circle distance given by

$$s = R \arccos\left[\cos\phi\cos\phi_f \cos(\theta-\theta_f)+\sin\phi\sin\phi_f\right] \tag{14}$$

where θ_f and ϕ_f are the longitude and latitude of the target, respectively, and the constant R is set to a (possibly local) mean surface radius. Then the terminal altitude and velocity condition are scored according to the weighted parachute box defined earlier. In the corrector step, the bank angle profile and M_{SIAD} are modified to maximize the score.

The bank angle magnitude profile is parameterized as a linear function given by [21]

$$|\sigma|(e)=\begin{cases}\sigma_f+\dfrac{|\sigma|_{\mathrm{c}}-\sigma_f}{e_{\mathrm{c}}-e_f}(e-e_f), & \text{if } e>e_f\\ \sigma_f, & \text{if } e\le e_f\end{cases} \tag{15}$$

where the specific energy e is defined by $e = v^2/2 - \mu/r$ with μ the Mars gravitational constant, e_c is the current energy, e_f is the terminal energy determined by the terminal altitude and velocity for point P, $|\sigma|_c$ is the current bank angle magnitude to be adjusted, and $\sigma_f > 0$ is the magnitude of the terminal bank angle. At the entry interface, e_c and $|\sigma|_c$ are equal to the initial energy e_0 and the magnitude of the initial bank angle $|\sigma|_0$, respectively. Limits for the bank angle magnitude $|\sigma|_c$ are

$$\sigma_{min} \le |\sigma|_c \le \sigma_{max} \tag{16}$$

where σ_{min} and σ_{max}, both positive, are the specified minimum and maximum bank angles, respectively; $\sigma_{min} = 10$ deg and $\sigma_{max} = 90$ deg are used for the numerical results. Note that the adjustment of $|\sigma|_c$ would no longer change the bank profile in Eq. (15) when $e_c \le e_f$. In that case, σ_f is used as a guidance parameter instead of $|\sigma|_c$.

Given the bank angle profile, the trajectory is integrated using the fourth-order Runge-Kutta method. The corrector adjusts $|\sigma|_c$ and/or M_{SIAD}, within their allowed intervals, such that the maximum score is achieved. The maximization problem is expressed as

$$\max C[\mathrm{T}(|\sigma|_c, M_{SIAD})] \tag{17}$$

indicating the dependence of the predicted terminal condition T on $|\sigma_c|$ and M_{SIAD}.

The corrector design considers the following. The number of longitudinal guidance parameters adjusted at any given time should be small, ideally one, to simplify and increase the reliability of the onboard computation. In the hypersonic phase, bank angle adjustments are preferred over M_{SIAD} adjustments, because the former have an immediate effect. The control authority offered by M_{SIAD} adjustments should be reserved for the latter portion of the hypersonic phase. Just prior to entering the interval of allowed Mach numbers for SIAD deployment, the focus should be on M_{SIAD}. Once the SIAD has been deployed, $|\sigma|_c$ is the only effective guidance parameter.

Consistent with the considerations just described, the guidance approach has the three phases defined in Table 1. (Although not accounted for explicitly, it is assumed that there would be an attitude-hold pre-bank phase, prior to guidance initiation, during early entry when aerodynamic forces are too small to affect the flight path significantly; see [30] for example.) In Phase 1, M_{SIAD} is fixed at the nominal value M_{nom} , and $|\sigma|_c$ is adjusted by the predictor-corrector algorithm. In Phase 2, M_{SIAD} is adjusted and $|\sigma|_c$ is fixed at value at the end of Phase 1. When the actual Mach number decreases to M_{SIAD} given by the guidance algorithm, the SIAD deploys. In Phase 3, $|\sigma|_c$ is adjusted until the parachute is deployed according to the range trigger. Accordingly, the guidance commands are

$$\begin{cases} \text{Phases 1 and 3:} & |\sigma|_c^{\text{command}} = \arg\max_{|\sigma|_c} C[\mathrm{T}(|\sigma|_c, M_{\text{SIAD}})] \\ \text{Phase 2:} & M_{\text{SIAD}}^{\text{command}} = \arg\max_{M_{\text{SIAD}}} C[\mathrm{T}(|\sigma|_c, M_{\text{SIAD}})] \end{cases} \tag{18}$$

where $|\sigma|_c$ is restricted to the interval of $[\sigma_{\min}, \sigma_{\max}]$, and M_{SIAD} is restricted to the interval bounded by the current Mach number and $M_{\min}$. A one-parameter search problem must be solved in each of the three phases. In this study, the golden section search method is employed. Note that the command $|\sigma|_c^{\text{command}}$ needs to be combined with the lateral guidance logic, which determines the sign of the bank angle, to generate the bank angle command. The SIAD deployment command is executed when the current Mach number is not greater than M_{SIAD} and a bank reversal is not in progress. During a bank reversal, the SIAD deployment is delayed until the reversal is complete.

Table 1 Corrector Phases

Phase	Mach	SIAD	$\|\sigma\|_c$	M_{SIAD}
1	$> M_{\max}$	undeployed	corrected	M_{nom}
2	$[M_{\text{SIAD}}, M_{\max}]$	undeployed	fixed	corrected
3	$< M_{\text{SIAD}}$	deployed	corrected	fixed

IV. Guidance Performance

A. Simulation Conditions and Error Modeling

The proposed guidance method is assessed for an MSL-type vehicle with a SIAD. Diameters for the aeroshell and SIAD are 4.5 m and 6.0 m, respectively. Together with the SIAD mass which is about 100 kg [2], the vehicle's total mass is assumed to be 4500 kg. Compared with the MSL entry vehicle whose mass is 3300 kg, this vehicle is heavier consistent with the use of the SIAD is to accommodate larger payloads.

The guidance algorithm is tested with the update rate of 1 Hz. The linear bank angle profile is initialized with $|\sigma|_0$ = 70 deg and σ_f = 45 deg. The bank angle limits are $\sigma_{\max}$ = 90 deg and $\sigma_{\min}$ = 10 deg. The maximum bank angle rate and acceleration are 20 deg and 5 deg/s^2, respectively. The nominal SIAD deployment Mach number is M_{nom} = 4, and the limits are $M_{\max}$ = 5 and $M_{\min}$ = 3.

The initial entry conditions and the dispersions (3 standard deviations) are given in Table 2 [12]. The target's position is θ_f = -73.26 deg and ϕ_f = -41.45 deg. The nominal parachute deployment condition is h_f = 8.6 km and v_f =

410 m/s. Perfect onboard state information is assumed; i.e., navigation error is neglected. The atmospheric density is modeled by

$$\rho = (1+\Delta\rho)\rho_0 \exp(-h/h_s) \tag{19}$$

where $\Delta\rho$ is the density dispersion, $\rho_0 = 0.0158$ kg/m^3 is the nominal density on Mars surface, and $h_s = 9354.5$ m is the nominal density scale height [29]. The dispersion $\Delta\rho$ changes with the altitude. The vehicle lift and drag coefficients are modeled by

$$\begin{cases} C_L = (1+\Delta C_L)C_L^* \\ C_D = (1+\Delta C_D)C_D^* \end{cases} \tag{20}$$

where ΔC_L and ΔC_D are dispersions of the lift and drag coefficients, respectively. The nominal values C_L^* and C_D^* are both functions of the Mach number [31].

Table 2 Initial conditions and dispersions for Mars entry

Parameter	Mean	3 standard deviations
Altitude (km)	123	2.306
Velocity (m/s)	5505	2.85
Flight-path angle (deg)	-14.15	0.15
Longitude (deg)	-90.072	0.3
Latitude (deg)	-43.898	0.03
Heading angle (deg)	4.99	0.23

Note that Eqs. (2-7) combined with Eqs. (19) and (20) are used for both the predictor model and the truth dynamics. Here truth dynamics, which are used in the performance assessment, are the dynamics based on vehicle and environmental models that account for various off-nominal conditions. In integrating the truth dynamics, the range trigger assumed in the predictor-corrector algorithm terminates the trajectory at the position where the parachute would be deployed. For the predictor model, the aerodynamic dispersions are unknown, and we set $\Delta\rho = 0$, $\Delta C_L = 0$, and $\Delta C_D = 0$ in Eqs. (19) and (20) consistent with the nominal model. In contrast, for the truth dynamics, dispersions are nonzero (except for the nominal case).

In the subsequent subsections, the guidance method is firstly tested in the nominal case with $\Delta\rho = 0$, $\Delta C_L = 0$, $\Delta C_D = 0$, and no delivery error for the entry state. Then, with the delivery error and aerodynamic errors, 500 dispersed cases are considered to assess the guidance method. In the dispersed cases, the altitude-dependent density dispersion $\Delta\rho$, as shown in Fig. 4, is given by the Mars Climate Database [32]. For each case, the aerodynamic

dispersions ΔC_L and ΔC_D are assumed constant and take values from a zero-mean Gaussian distribution with 3 standard deviations of 0.1. Note that the 500 dispersed conditions are generated once and then utilized in each of the tests under dispersions.

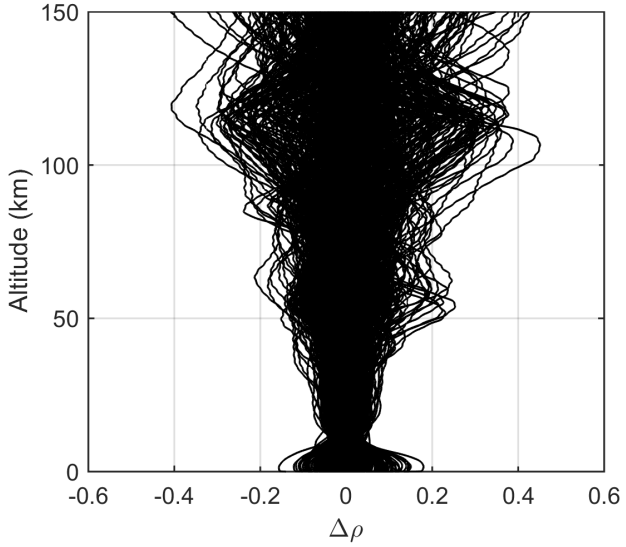

Fig. 4 Atmospheric density dispersions (500 cases)

B. Nominal Case

For the nominal case described above, the ground track of the guided entry trajectory is shown in Fig. 5(a). The target is reached accurately with a 0.14 km horizontal position error (i.e., the horizontal distance between the vehicle's final position and the target). Figure 5(b) illustrates the bank angle history. Four bank reversals are employed during the entry flight. The drag acceleration is shown in Fig. 5(c); an obvious perturbation occurs when the SIAD deploys. The guidance command for the deployment Mach number M_{SIAD} remains 4 which is the initialized nominal value. This means that $M_{\mathrm{SIAD}} = 4$ maximizes C (T) consistently and no modification is required for the nominal case. The trajectory in the velocity versus altitude plane is illustrated in Fig. 5(d). The trajectory ends in the parachute deployment box with a score $C = 0.94$.

According to the guidance strategy, the bank angle $|\sigma|_{\mathrm{c}}$ is adjusted in Phases 1 and 3, while M_{SIAD} is adjusted in Phase 2. To calculate the adjustment for either $|\sigma|_{\mathrm{c}}$ or M_{SIAD}, a one-parameter search problem is solved to maximize the scoring function C. The scoring function at the beginning of each phase is shown in Fig. 6. The function is unimodal, and thus the golden section search method is effective in solving the maximization problem. At the beginning of Phase 1, the scoring function varies over a larger interval of values, because the modification of $|\sigma|_{\mathrm{c}}$ changes the whole bank profile. In contrast, the scoring function varies much less at the beginning of Phase 3

because changing $|\sigma|_c$ has less impact. At the beginning of Phase 2, note that the maximum score appears at $M_{\mathrm{SIAD}} = 4$.

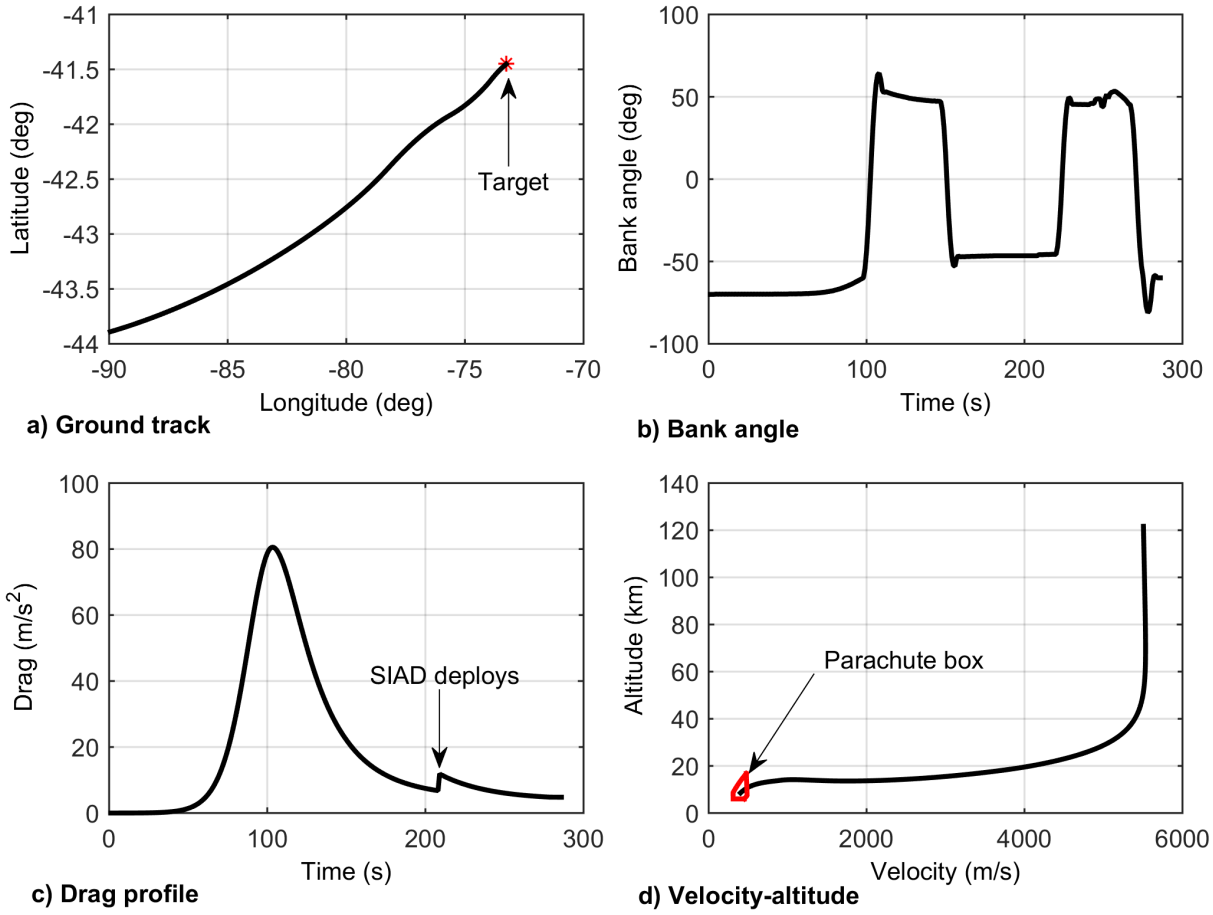

Fig. 5 Simulation results for the nominal case

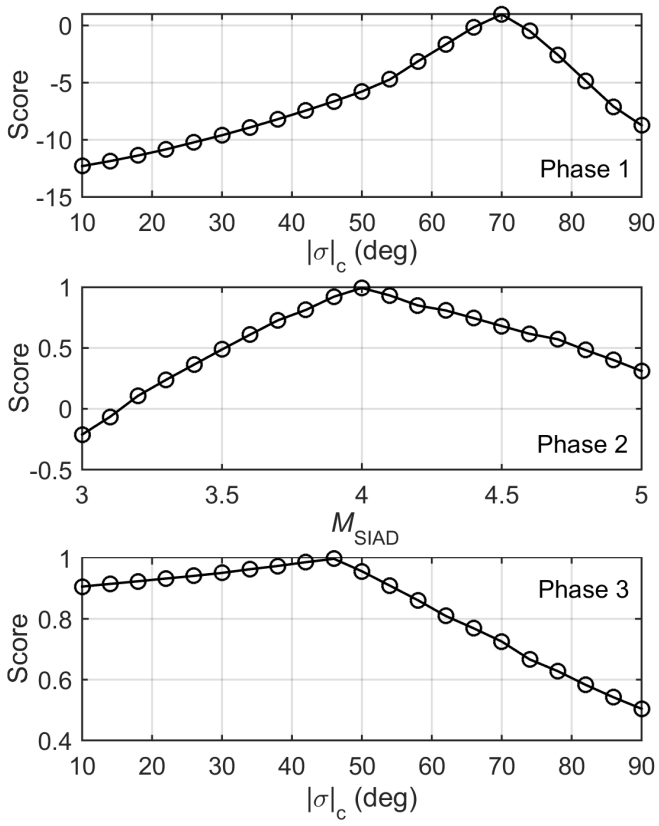

Fig. 6 Scoring function at the beginning of each phase

C. Variation with Vehicle Mass

The guidance performance for a range of payload masses is investigated. In addition to the nominal case, another five cases are considered with total vehicle masses of 3000 kg, 4000 kg, 5000 kg, 6000 kg, and 7000 kg. Cases 1 and 2 have smaller payloads relative to the nominal case, while Cases 3-5 have larger payloads. With respect to the nominal case, Cases 1 and 5 have the minimum and maximum mass differences of -33% and 56%.

The proposed guidance is tested for the five masses with all other conditions nominal. The simulation results are given in Table 3. For a higher mass, a larger M_{SIAD} is utilized to lengthen the flight time with higher deceleration. Scores for the five cases are all positive, which means that the parachute constraints are satisfied. Moreover, in each case the score is greater than 0.6 indicating the parachute deployment condition is not near a constraint boundary, i.e., there is a safety margin. The horizontal position error is within 1 km, indicating the effectiveness of the range-trigger and the lateral guidance logic. Figure 7 illustrates velocity-altitude trajectories for the five cases. The lower the mass is, the higher the vehicle flies. These results demonstrate that the guidance method, which modifies M_{SIAD} onboard, is applicable to a range of vehicle masses when the other conditions are nominal.

Table 3 Results for different vehicle masses

Case	Mass	M_{SIAD}	Score	Horizontal position error
1	3000 kg	3.58	0.88	0.10 km
2	4000 kg	3.73	0.97	0.22 km
3	5000 kg	4.18	0.96	0.44 km
4	6000 kg	4.52	0.79	0.44 km
5	7000 kg	4.82	0.61	0.65 km

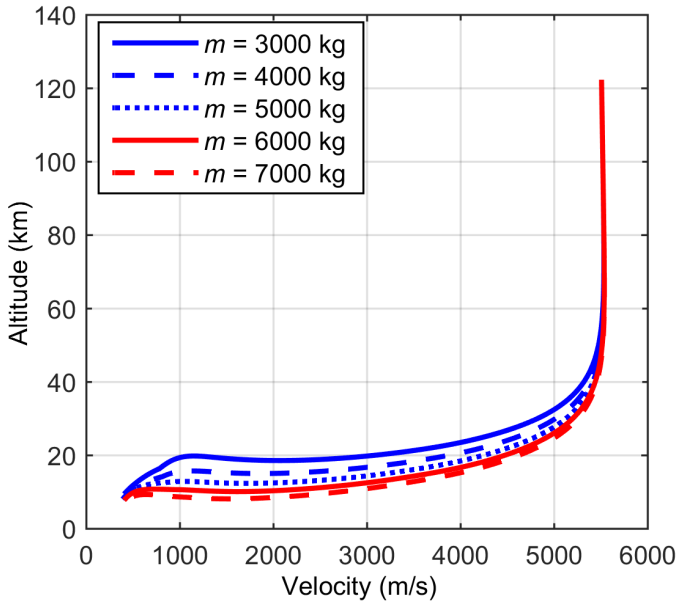

Fig. 7 Velocity-altitude trajectories for various vehicle masses

D. Dispersed Cases

The guidance performance under dispersions is assessed next. Altitude-velocity trajectories for the 500 dispersed cases are shown in Fig. 8. The final parachute deployment constraint is well satisfied. For all the cases, the score is higher than 0.4. Figure 9 illustrates terminal locations for the entry phase. Under the lateral guidance logic and the range-trigger, the horizontal position errors are within 1 km for all the cases. Therefore, the predictor-corrector guidance algorithm is demonstrated to be robust to entry dispersions.

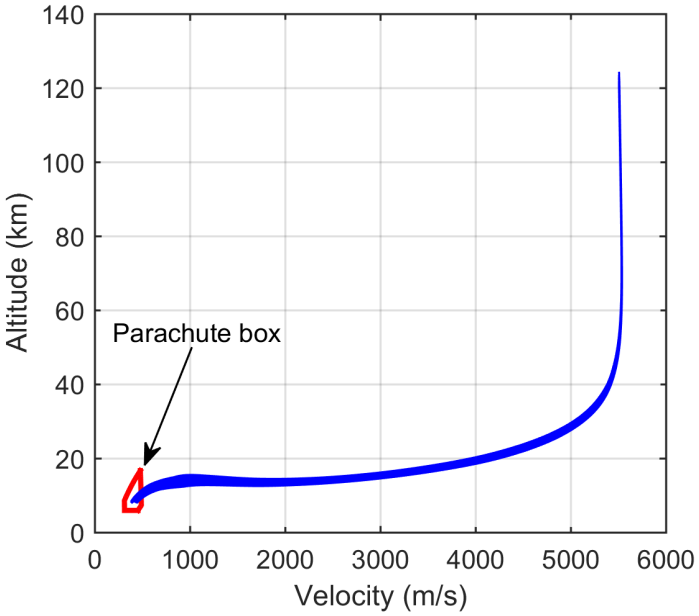

Fig. 8 Velocity-altitude trajectories for 500 dispersed cases

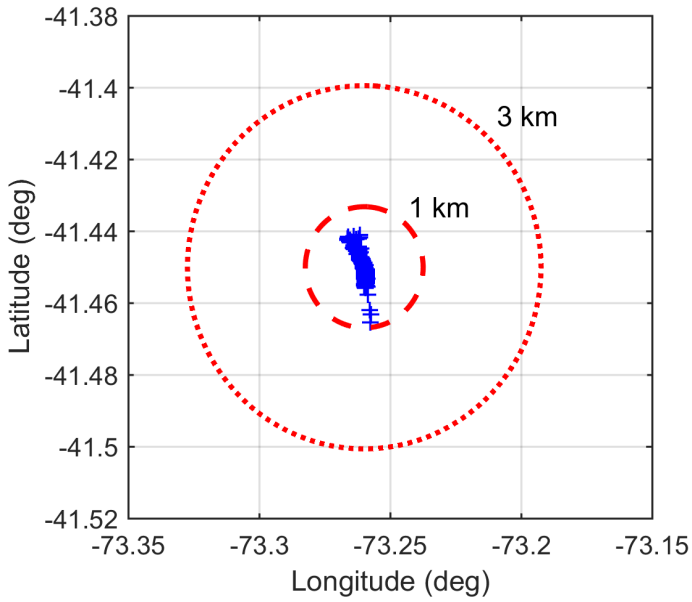

Fig. 9 Terminal locations for 500 dispersed cases

E. Variation with Number of Guidance Parameters Corrected

The proposed guidance method utilizes two guidance parameters, the bank angle $|\sigma|_c$ and the Mach number M_{SIAD}. In the third phase, after the SIAD has been deployed, only the bank angle can be adjusted. As for the first and the second phases, both $|\sigma|_c$ and M_{SIAD} could be adjusted. According to the proposed corrector strategy tested in the previous subsection, a single guidance parameter is adjusted in each phase. In order to assess the effect of

restricting the corrector to one parameter at a time, further testing is conducted. The proposed strategy, named Strategy 1, is compared with two other strategies defined as follows.

Strategy 1: Adjust $|\sigma|_c$ for Phase 1, and adjust M_{SIAD} for Phase 2.

Strategy 2: Adjust $|\sigma|_c$ for Phase 1, and adjust $|\sigma|_c$ and M_{SIAD} for Phase 2.

Strategy 3: Adjust $|\sigma|_c$ and M_{SIAD} for Phases 1 and 2.

For Strategies 2 and 3, when the two guidance parameters must be determined simultaneously, the gradient method is employed. These two strategies are both tested in the dispersed cases considered earlier. The horizontal position error is acceptable for all the trajectories. Scores are calculated for the parachute deployment condition, and the mean score is obtained from the results of the 500 cases. For Strategies 1-3, the mean scores are 0.88, 0.86, and 0.87, respectively. Therefore, in respect of robustness, Strategy 1 is no worse, and sometimes even better, than the other two.

The simulation in this study is conducted on a PC (CPU: 2.6 GHz) using the software of MATLAB R2014b. The computation time (measured by the "tic-toc" function) taken by the guidance algorithm in each cycle is recorded. The maximum computation time for the three strategies is compared in Table 4. The maximum time always occurs in the initial flight phase where the whole entry trajectory needs to be predicted. Hence, Strategy 3 which calculates two guidance parameters takes the longest time in Phase 1. As for Phase 2, since both Strategies 2 and 3 calculate two parameters, Strategy 1 takes the shortest time. According to the maximum computation time for the whole flight, Strategy 1 performs better than Strategy 2, and similarly to Strategy 3. Note that the computational performance depends on the search method used for the guidance parameter update. The computation time can likely be reduced by using a more efficient search method.

Apart from the robustness and the real-time performance, the reliability is also a concern. Generally, Strategy 1 is more reliable because it adjusts one parameter in each guidance cycle. Therefore, synthesizing the robustness, the real-time performance, and the reliability, Strategy 1 is a better choice than Strategies 2 and 3.

Table 4 Maximum computation time for Strategies 1-3

Strategy	Phase 1	Phase 2	Whole Flight
1	0.21 s	0.08 s	0.21 s
2	0.21 s	0.19 s	0.21 s
3	0.55 s	0.19 s	0.55 s

F. Variation with SIAD Deployment Mach Number

In the proposed guidance method, the allowable M_{SIAD} interval is [3.0, 5.0]. To determine how the size of the Mach number interval [M_{SIAD}] impacts the guidance performance, results for four Mach number intervals are compared.

$[M_{SIAD}]_1 = [4.0, 4.0]$, i.e., $M_{SIAD} = 4$, non-adjustable.

$[M_{SIAD}]_2 = [3.7, 4.3]$.

$[M_{SIAD}]_3 = [3.3, 4.7]$.

$[M_{SIAD}]_4 = [3.0, 5.0]$.

The four Mach intervals $[M_{SIAD}]_{1\text{-}4}$ are tested in the 500 dispersed cases. Because the range trigger and the bank reversal logic are used for each, the four methods achieve similar accuracy for the terminal location. The parachute deployment conditions for $[M_{SIAD}]_{1\text{-}4}$ are shown in Fig. 10. Scores are calculated based on the weighted parachute box. The mean scores for $[M_{SIAD}]_{1\text{-}4}$ are 0.80, 0.86, 0.87, and 0.88, respectively. With the Mach number modification, $[M_{SIAD}]_{2\text{-}4}$ achieve higher scores than $[M_{SIAD}]_1$. In addition, the box boundary corresponding to $C = 0.5$ is plotted in Fig. 10. For $[M_{SIAD}]_1$, 23 cases have scores lower than 0.5. For $[M_{SIAD}]_2$, the case number of $C < 0.5$ is reduced to 5. With higher Mach number modification interval, $[M_{SIAD}]_3$ and $[M_{SIAD}]_4$ both reduce the number to 1. Therefore, a larger Mach number modification interval is demonstrated to be effective to achieve a better deployment condition for the parachute.

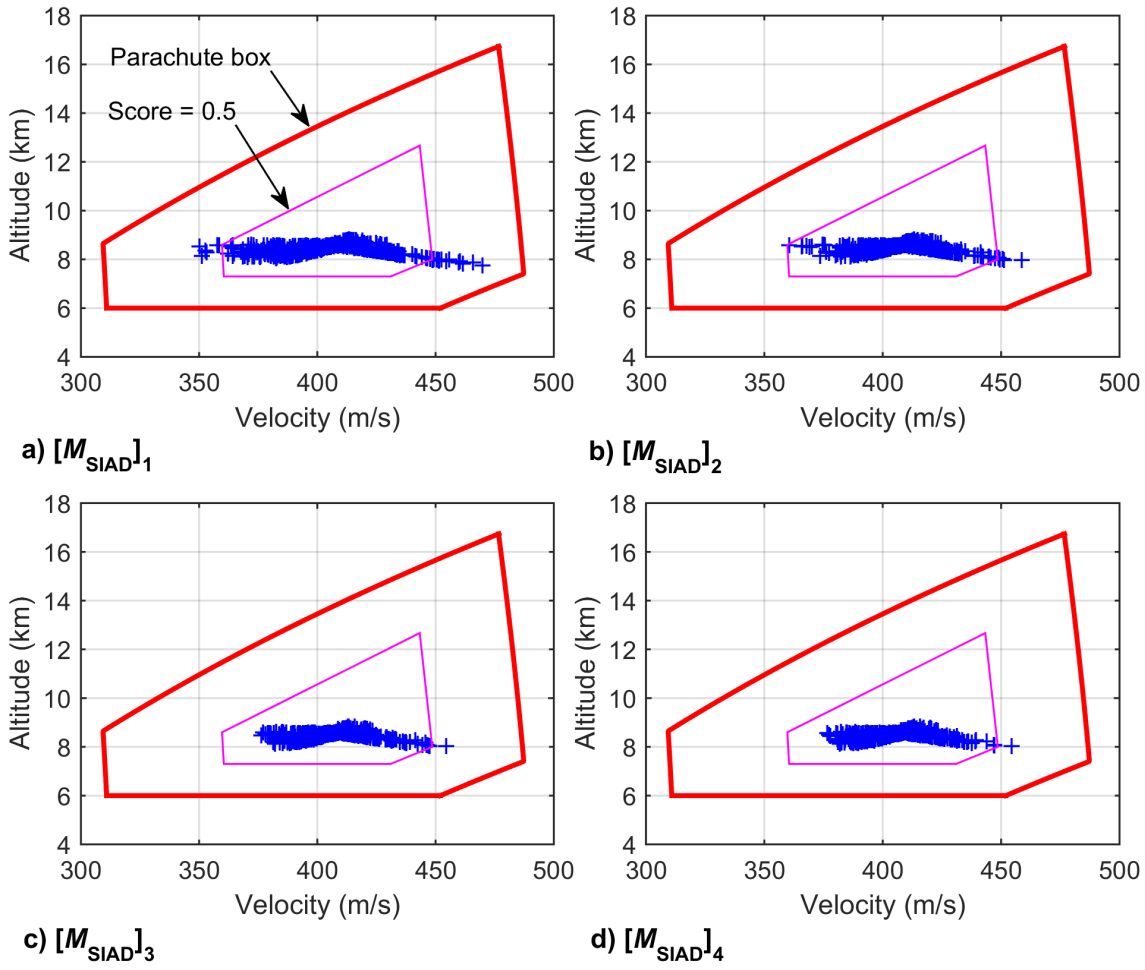

Fig. 10 Parachute deployment conditions in dispersed cases

V. Conclusions

The supersonic inflatable aerodynamic decelerator (SIAD) is being considered for future Mars landing missions with heavier payloads. A guidance method for Mars entry with the SIAD has been proposed and its performance assessed. A numerical predictor-corrector algorithm is used for longitudinal guidance to achieve a delivery state that meets the horizontal position and parachute deployment requirement. In addition to the bank angle magnitude, the SIAD deployment Mach number is used as a longitudinal guidance parameter. The entry flight is divided into three phases, and a single guidance parameter is adjusted by the corrector in each phase. The lateral guidance is the previously developed bank reversal logic and commands the sign of the bank angle. Simulation results indicate that the proposed guidance is effective for Mars entry with a SIAD. A Mars Science Laboratory type vehicle with various masses from 3000 kg to 7000 kg was considered. Entry trajectories were successfully flown for the vehicle deploying the SIAD at a higher Mach number for a higher mass. The horizontal position delivery error can be

controlled to within 1 km, and the altitude and velocity at delivery satisfy the requirements for parachute deployment with a margin of safety. The impact of the allowed variation in the deployment Mach number on the guidance performance was investigated; the results showed that better performance is achieved when larger variation is allowed.

References

[1] Braun, R. D., and Manning, R. M., "Mars Exploration Entry, Descent, and Landing Challenges," *Journal of Spacecraft and Rockets,* Vol. 44, No. 2, 2007, pp. 310-323.
doi: 10.2514/1.25116

[2] Clark, I. G., Hutchings, A. L., Tanner, C. L., and Braun, R. D., "Supersonic Inflatable Aerodynamic Decelerators for Use on Future Robotic Missions to Mars," *Journal of Spacecraft and Rockets,* Vol. 46, No. 2, 2009, pp. 340-352.
doi: 10.2514/1.38562

[3] Clark, I. G., Rivellini, T., and Adler, M., "Development and Testing of a New Family of Low-Density Supersonic Decelerators," *AIAA Aerodynamic Decelerator Systems (ADS) Conference*, AIAA Paper 2013-1252, 2013.
doi: 10.2514/6.2013-1252

[4] Smith, B., Hill, J., Clark, I., and Braun, R., "Oscillation of Supersonic Inflatable Aerodynamic Decelerators at Mars," *21st AIAA Aerodynamic Decelerator Systems Technology Conference and Seminar*, AIAA Paper 2011-2516, 2011.
doi: 10.2514/6.2011-2516

[5] Giersch, L., Rivellini, T., Clark, I. G., Sandy, C., Sharpe, G., Shook, L. S., Ware, J. S., Welch, J., Mollura, J., and Dixon, M., "SIAD-R: A Supersonic Inflatable Aerodynamic Decelerator for Robotic Missions to Mars," *AIAA Aerodynamic Decelerator Systems (ADS) Conference*, AIAA Paper 2013-1327, 2013.
doi: 10.2514/6.2013-1327

[6] Bose, D. M., Shidner, J., Winski, R., Zumwalt, C., Cheatwood, F. M., and Hughes, S. J., "The Hypersonic Inflatable Aerodynamic Decelerator (HIAD) Mission Applications Study," *AIAA Aerodynamic Decelerator Systems (ADS) Conference*, AIAA Paper 2013-1389, 2013.
doi: 10.2514/6.2013-1389

[7] Clark, I. G., Manning, R., and Adler, M., "Summary of the First High-Altitude, Supersonic Flight Dynamics Test for the Low-Density Supersonic Decelerator Project," *23rd AIAA Aerodynamic Decelerator Systems Technology Conference*, AIAA Paper 2015-2100, 2015.
doi: 10.2514/6.2015-2100

[8] Giersch, L., Shook, L., Tanimoto, R., and Blood, E., "Supersonic Flight Test of the SIAD-R: Supersonic Inflatable Aerodynamic Decelerator for Robotic Missions to Mars," *23rd AIAA Aerodynamic Decelerator Systems Technology Conference*, AIAA Paper 2015-2135, 2015.
doi: 10.2514/6.2015-2135

[9] O'Farrell, C., Brandeau, E. J., Tanner, C., Gallon, J. C., Muppidi, S., and Clark, I. G., "Reconstructed Parachute System Performance During the Second LDSD Supersonic Flight Dynamics Test," *AIAA Atmospheric Flight Mechanics Conference*, AIAA Paper 2016-3242, 2016.
doi: 10.2514/6.2016-3242

[10] Tu, K.-Y., Munir, M. S., Mease, K. D., and Bayard, D. S., "Drag-Based Predictive Tracking Guidance for Mars Precision Landing," *Journal of Guidance, Control, and Dynamics,* Vol. 23, No. 4, 2000, pp. 620-628.

doi: 10.2514/6.1998-4573

[11] Kluever, C., "Entry Guidance Performance for Mars Precision Landing," *Journal of Guidance, Control, and Dynamics,* Vol. 31, No. 6, 2008, pp. 1537-1544.
doi: 10.2514/1.36950

[12] Benito, J., and Mease, K. D., "Nonlinear Predictive Controller for Drag Tracking in Entry Guidance," *AIAA/AAS Astrodynamics Specialist Conference and Exhibit*, AIAA Paper 2008-7350, 2008.
doi: 10.2514/6.2008-7350

[13] Dai, J., and Xia, Y., "Mars Atmospheric Entry Guidance for Reference Trajectory Tracking," *Aerospace Science and Technology,* Vol. 45, 2015, pp. 335-345.
doi: 10.1016/j.ast.2015.06.006

[14] Liang, Z., Duan, G., and Ren, Z., "Mars Entry Guidance Based on an Adaptive Reference Drag Profile," *Advances in Space Research,* Vol. 60, No. 3, 2017, pp. 692-701.
doi: 10.1016/j.asr.2017.04.027

[15] Youssef, H., Chowdhry, R., Lee, H., Rodi, P., and Zimmermann, C., "Predictor-Corrector Entry Guidance for Reusable Launch Vehicles," *AIAA Guidance, Navigation, and Control Conference*, AIAA Paper 2001-4043, 2001.
doi: 10.2514/6.2001-4043

[16] Joshi, A., Sivan, K., and Amma, S. S., "Predictor-Corrector Reentry Guidance Algorithm with Path Constraints for Atmospheric Entry Vehicles," *Journal of Guidance, Control, and Dynamics,* Vol. 30, No. 5, 2007, pp. 1307-1318.
doi: 10.2514/1.26306

[17] Lu, P., "Predictor-Corrector Entry Guidance for Low-Lifting Vehicles," *Journal of Guidance, Control, and Dynamics,* Vol. 31, No. 4, 2008, pp. 1067-1075.
doi: 10.2514/1.32055

[18] Putnam, Z. R., and Braun, R. D., "Precision Landing at Mars Using Discrete-Event Drag Modulation," *Journal of Spacecraft and Rockets,* Vol. 51, No. 1, 2014, pp. 128-138.
doi: 10.2514/1.A32633

[19] Putnam, Z. R., Clark, I. G., and Braun, R. D., "Drag Modulation Flight Control for Aerocapture," *IEEE Aerospace Conference*, IEEE, 2012.
doi: 10.1109/AERO.2012.6186999

[20] Putnam, Z. R., and Braun, R. D., "Drag-Modulation Flight-Control System Options for Planetary Aerocapture," *Journal of Spacecraft and Rockets,* Vol. 51, No. 1, 2014, pp. 139-150.
doi: 10.2514/1.a32589

[21] Lu, P., "Entry Guidance: A Unified Method," *Journal of Guidance, Control, and Dynamics,* Vol. 37, No. 3, 2014, pp. 713-728.
doi: 10.2514/1.62605

[22] Lu, P., Brunner, C. W., Stachowiak, S. J., Mendeck, G. F., Tigges, M. A., and Cerimele, C. J., "Verification of a Fully Numerical Entry Guidance Algorithm," *Journal of Guidance, Control, and Dynamics,* Vol. 40, No. 2, 2017, pp. 230-247.
doi: 10.2514/1.g000327

[23] Zheng, Y., Cui, H., and Ai, Y., "Constrained Numerical Predictor–Corrector Guidance for Mars Precision Landing," *Journal of Guidance, Control, and Dynamics,* Vol. 40, No. 1, 2017, pp. 177-185.
doi: 10.2514/1.g000563

[24] Harpold, J., "Shuttle Entry Guidance," *Journal of Astronautical Sciences,* Vol. 27, No. 3, 1979, pp. 239-268.

[25] Way, D., "On the Use of a Range Trigger for the Mars Science Laboratory Entry, Descent, and Landing," *2011 IEEE Aerospace Conference*, 2011.
doi: 10.1109/AERO.2011.5747242

[26] Mendeck, G. F., and Carman, G. L., "Guidance Design for Mars Smart Landers Using the Entry Terminal Point Controller," *AIAA Atmospheric Flight Mechanics Conference and Exhibit*, AIAA Paper 2002-4502, 2002. doi: 10.2514/6.2002-4502

[27] Dutta, S., and Way, D. W., "Comparison of the Effects of Velocity and Range Triggers on Trajectory Dispersions for the Mars 2020 Mission," *AIAA Atmospheric Flight Mechanics Conference*, 2017. doi: 10.2514/6.2017-0245

[28] Vinh, N. X., Busemann, A., and Culp, R. D., *Hypersonic and Planetary Entry Flight Mechanics*, Univ. of Michigan Press, Ann Arbor, MI, 1980, pp. 26-28.

[29] Benito, J., and Mease, K. D., "Reachable and Controllable Sets for Planetary Entry and Landing," *Journal of Guidance, Control, and Dynamics,* Vol. 33, No. 3, 2010, pp. 641-654. doi: 10.2514/1.47577

[30] Prakash, R., Burkhart, D., Chen, A., Comeaux, K. A., Guernsey, C. S., Kipp, D. M., Lorenzoni, L. V., Mendeck, G., Powell, R., Rivellini, T., Martin, M. S., Sell, S. W., Steltzner, A., and Way, D., "Mars Science Laboratory Entry, Descent, and Landing System Overview," *IEEE Aerospace Conference*, IEEE, 2010. doi: 10.1109/AERO.2008.4526283

[31] Benito, J., "Advances in Spacecraft Atmospheric Entry Guidance," University of California, Irvine, 2010.

[32] Millour, E., Forget, F., and Lewis, S. R., "Mars Climate Database V5.2 User Manual," 2015.